Graphical Abstract

A polygon model of the functional base-of-support improves the accuracy of balance analysis

Matthew Millard, Lizeth H. Sloot

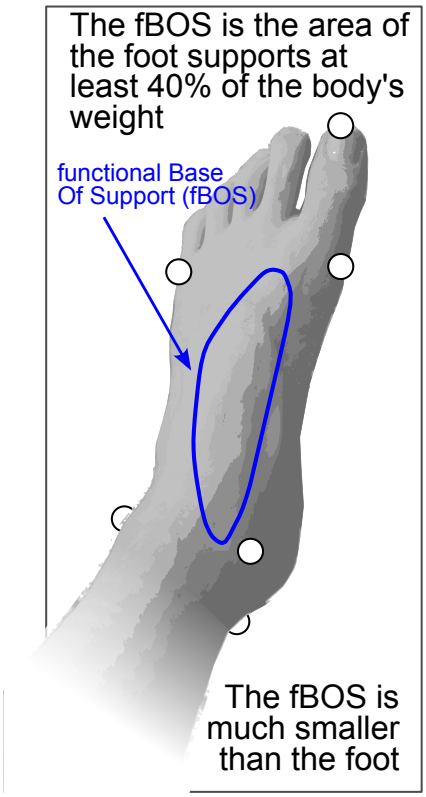

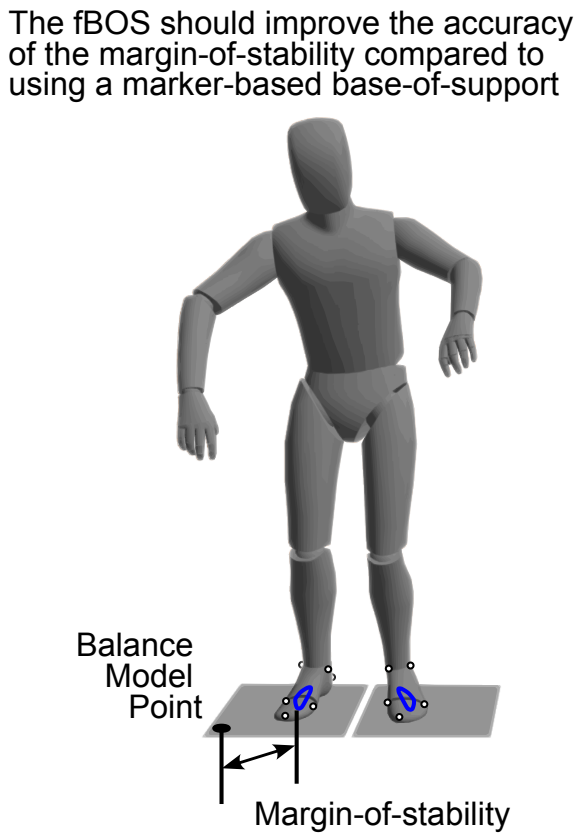

Highlights

A polygon model of the functional base-of-support improves the accuracy of balance analysis

Matthew Millard, Lizeth H. Sloot

- Only a small area of the foot, the functional–base-of-support (fBOS), can support at least 40% of the body's weight
- The fBOS can be measured using motion capture, force plates and a balancing task
- fBOS size is unaffected by footwear, stance width, and foot-dominance but varies between single and double stance
- Balance analysis accuracy should be improved by using the fBOS to evaluate the margin-of-stability

A polygon model of the functional base-of-support improves the accuracy of balance analysis

Matthew Millard[a,b,1], Lizeth H. Sloot[c,d]

[a] *University of Stuttgart, Institute of Sport and Movement Sciences, Stuttgart, 70180, BW, Germany*
[b] *University of Stuttgart, Institute of Engineering and Computational Mechanics, Stuttgart, 70180, BW, Germany*
[c] *Newcastle University, Translational and Clinical Research Institute, Newcastle, Newcastle upon Tyne, NE1 7RU, UK*
[d] *University Heidelberg, Institute of Computer Engineering, Heidelberg, BW, 69120, Germany*

Abstract

Mathematical balance models have the potential to identify people at risk of falling before an injury occurs. However, most balance models depend on a model of the base-of-support (BOS) of the feet to calculate how well someone is balancing. Here we evaluate the functional base-of-support (fBOS): the convex polygon on the bottom of the foot that can support a large fraction of the body's weight. First, we develop a geometric model of the fBOS by measuring the center-of-pressure (COP) and kinematic data of the feet of 27 younger adults instructed to move their body mass in large loops without taking a step. We extract a planar convex polygon that contains the COP data. Finally, we compare the area of this fBOS model to a marker-based BOS model before evaluating if the fBOS differs across four everyday conditions: footwear, stance-width, foot dominance, and during single and double stance. We found that the fBOS is much smaller (23% the size) than a marker-based BOS model. Our analysis suggests that using the fBOS, rather than a marker-based BOS, can improve the accuracy of the margin-of-stability by 20% of foot width and 16% of the length. In addition, we found that the fBOS area does not differ across footwear ($p = 0.88$), stance-width ($p = 0.88$), and foot dominance ($p = 0.68$), but during single stance the fBOS is 17% ($p = 0.0003$) larger than during double stance. So that others can use and extend our work, we have made the models, example data and code publicly available.

Email addresses: matthew.millard@inspo-stuttgart.de (Matthew Millard), lizeth.sloot@newcastle.ac.uk (Lizeth H. Sloot)

[1] equal authors

Keywords: Base-Of-Support, Balance, Stability, Center-Of-Pressure, Foot Placement Estimator, Extrapolated Center of Mass, Margin-of-Stability

1. Introduction

Older adults often fall during everyday movements such as walking. Balance is a complex skill of coordinating the body's movements and foot placements to move efficiently and safely. Models of dynamic balance Hof (2008); Kajita and Tani (1991); Millard et al. (2012) simplify balance analysis by mapping the body's movements to a point on the floor: if that balance point can be covered by the base of support (BOS) the model can be considered balanced, otherwise action needs to be taken to prevent a fall. Balance studies generally report the margin-of-stability, which is the distance between a person's balance point Hof (2008); Kajita and Tani (1991); Millard et al. (2012) and the nearest edge of their BOS. The margin-of-stability is a useful metric for assessing balance performance, but its accuracy depends on the accuracy of the BOS.

A recent literature review on the margin-of-stability in pathological gait shows that there is no standardized definition of the BOS Watson et al. (2021). Instead, lateral BOS boundaries were based on lateral toe markers (n=7), lateral malleolus or shoe markers (n=6) or the position of the center-of-pressure (COP; n=7). Similarly, the anterior or posterior BOS boundaries were defined using a marker on the toe (n = 8), the malleolus of the ankle (n = 3) or the heel (n = 3). Not only do these changing marker-based definitions limit the ability to compare between studies, but these definitions likely give an inaccurate estimate of the BOS area. Our previous work Sloot et al. (2020), shows that even changing from a multi-marker-based BOS model to a functional BOS (fBOS) model can reduce the variation of margin-of-stability data (from 1.8 cm to 1.4 cm in younger and 3.8 cm to 1.8 cm in older adults) making it possible to detect differences that previously were hidden (from $p = 0.633$ to $p = 0.004$).

The fBOS is the area of the foot that can support a large fraction of the body's weight. The edges of this area have been estimated during standing using the limits of stability test Melzer et al. (2004). During this test, the maximum COP excursion is measured as a person leans as much as possible in a specific direction without moving their feet. These evaluations show that, during standing, the edges of the fBOS are considerably smaller than

the entire footprint (or the anatomical outline of the foot) King et al. (1994). Studies have mostly limited their assessments in a singular direction, but a more recent study measured young persons leaning in eight different discrete directions Tomita et al. (2021).

As the fBOS has been evaluated primarily during standing barefoot, it remains unknown if the area depends on everyday factors such as footwear, stance width, foot dominance or varies between single and double stance. The stiffness of a shoe could provide extra support that increases the fBOS. A wider stance will change the joint angles and loads, which may in turn affect the fBOS area. The dominant foot may have a larger fBOS because of its better coordination and control in comparison to the non-dominant foot. Finally, during single stance, the fBOS may be smaller because of the increased load that the foot's musculature needs to resist. Understanding how the fBOS area is affected by these different factors is important for developing an fBOS model that is applicable to a wide variety of real-life scenarios.

In this paper, we first extend our preliminary fBOS model Sloot et al. (2020) by evaluating the fBOS of 27 young adults. Next, we compare the area of the fBOS to the area enclosed by a marker-based BOS model. Finally, we compute fBOS models across four different conditions to determine if the fBOS area is affected by footwear, stance width, foot dominance, and varies between single and double stance. In addition, we provide open-source scalable fBOS models that are applicable to movement data recorded using two common marker models (the IOR Leardini et al. (2007) and the PlugInGait model Vicon® (2002); Davis III et al. (1991); Grood and Suntay (1983)) with example code and data[2] so that others can build on our work.

2. Methods

Twenty-seven young able-bodied (27 ± 6 yr, 11 females, 23 ± 3 kg/m^2) participants were included in the study. Participants were excluded if they were not between 18 and 46 years of age, or had neurological, cardiovascular, metabolic, visual, auditory, mental or psychiatric impairments or injuries that might interfere with the planned task. Eighteen participants indicated their right foot as dominant. Two participants did not have a shod trial,

[2] `https://github.com/mjhmilla/functionalBaseOfSupport`

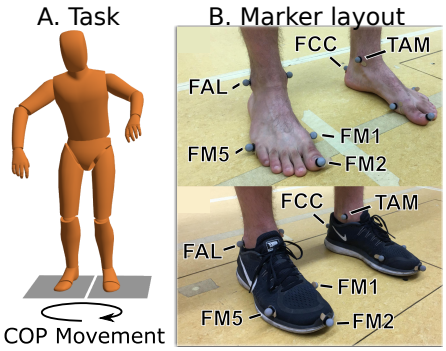

Figure 1: **Protocol and analysis**. A) Participants moved their center-of-pressure (COP) in large slow loops while not moving their feet, which were each positioned on a force plate hip-width apart (baseline condition). No instructions on arm movement or balance strategy were given. B) Marker placement for the barefoot and shod condition.

and four participants did not have the single foot and wide stance trials. The protocol was approved by the IRB of the medical faculty of Heidelberg University and the participants provided their written informed consent.

2.1. Protocol

To measure the fBOS, we had participants stand with each foot on a force plate and create the largest COP loop possible by moving their body in circles (Fig. 1A). Participants were asked to place their feet hip-width apart and complete the task without moving or lifting the heel or forefoot from the ground. They were not restricted in, or instructed on, arm movements or how best to lean in the different directions. Each participant was given as much time as needed and encouraged to make several circles until they felt satisfied with having produced the largest COP loop possible. The trial was repeated if a participant lost their balance before producing the largest COP loop possible. In addition, a quiet standing trial was also recorded and used to define the position and orientation of the bottom of the foot (the $\mathcal{K}_2$ in Figs. 2 B.5) when it is flat on the ground.

Participants repeated this task under different conditions so that we could see how the fBOS area is affected by footwear, stance width, foot dominance, and varies between single and double stance. Participants performed the task barefoot with the legs hip-width apart (baseline condition), with shoes, at a wider stance, and while standing on a single self-selected leg.

Foot movements and ground reaction forces were recorded while the participant slowly moved their COP. Foot movement was recorded using a motion capture system (150 Hz, type 5+ cameras, Qualisys, Gothenburg, Sweden) and ground reaction forces using two force plates (900 Hz, Bertec, Columbus, OH, USA). Motion capture markers (14mm) were placed on the heel, medial and lateral ankle epicondyles, first metatarsal (distal end, outside foot), fifth metatarsal (distal end, outside foot) - inspired by the IOR marker model Cappozzo et al. (1995); Leardini et al. (2011) - and on the tip of the most forward toe whether it was the first or second toe (Fig. 1B). Marker data were labeled in Qualisys and any data with marker dropout were excluded from analysis. We calculated the COP data from the force data. All kinematic and force-plate data were filtered with a bi-directional second-order low-pass Butterworth filter at half the marker sample frequency (75 Hz) and then down-sampled to the sampling rate of the motion capture system (150 Hz).

To exclude any COP data outliers that affected the analysis, we only included data from parts of a trial that met the following criteria: at least 150 consecutive data points (1 second) long, a substantial amount of weight on a single force plate, and the distance to neighboring data points was not among the largest 0.5% (deletion of outliers). During double-stance trial, we defined 40% of body weight as a substantial amount of weight, as 50% eliminated too much of the recorded data. By having a threshold lower than 50% we still included data from both feet from participants who naturally favoured one leg. Finally, data were only included if the foot was sufficiently flat on the ground.

We quantified how flat the foot was on the ground using the orientation of the bottom of the foot ($\mathcal{K}_2$ in Fig. 2 and B.5) relative to its orientation during quiet standing. We decomposed the orientation of $\mathcal{K}_2$ using a $\mathrm{X}(\psi_X) - \mathrm{Y}'(\theta_Y) - \mathrm{Z}''(\Psi_Z)$ Euler-axis decomposition. Thresholds for ψ_X and θ_Y were defined with the intention of identifying the angle at which a part of the foot loses contact with the ground. The foot is considered flat if $\mathrm{M} \sin \psi_X \leq 1.5\,\mathrm{cm}$ and $\mathrm{W} \sin \theta_Y \leq 1.5\mathrm{cm}$ where W and M are the width and mid-foot length of the foot (see Appendix A and Appendix B for details). We arrived at this threshold by noting that the heel Gefen et al. (2001) and second metatarsal foot pads compress an order of a centimetre Cavanagh (1999) under bodyweight, and increased the threshold upwards to include additional data in the analysis. The single threshold worked well for all participants except one who we excluded from this paper: this participant was able to

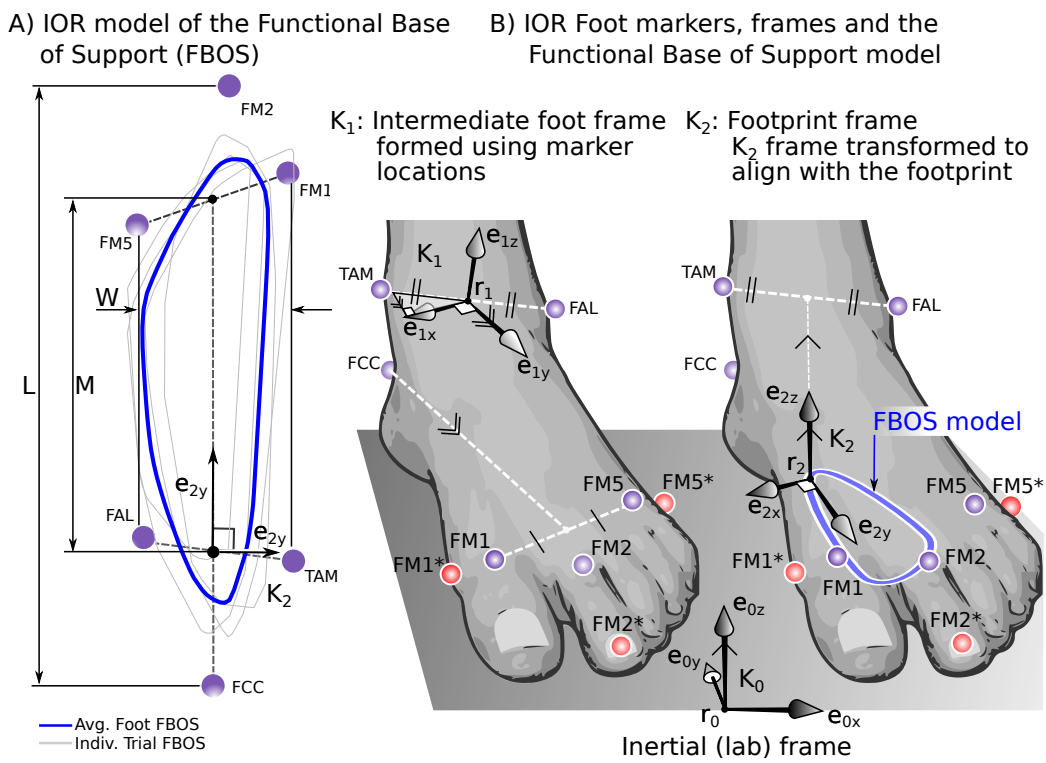

Figure 2: The fBOS is described as a series of points that define a convex polygon (A) in the frame $\mathcal{K}_2$ which is fixed to the foot. The foot's markers (B, left) are used to form frame $\mathcal{K}_1$ which is then transformed (B, right) using a pre-calculated offset vector and rotation matrix (see Appendix A and Appendix B for details). We made slight adjustments to the placement of the forefoot markers (shown in red) to have them on the side of the foot so that we could also use these marker positions to calculate the foot's width and length (A).

lift parts of their foot off the floor while meeting the 1.5cm threshold, and produced abnormally large fBOS areas as a result.

2.2. Functional Base-of-Support Model

We define the fBOS as the convex polygon (Fig. 2A) in the plane of the footprint that contains the area in which a participant can place at least 40% of their body weight while keeping their feet flat on the ground. The fBOS polygon (Fig. 2A) is created for each participant by projecting the COP data into the $\underline{e}_{2x} - \underline{e}_{2y}$ plane of the foot (Fig. 2B, see Appendix A

and Appendix B for details) and evaluating the convex hull that surrounds these COP points. A single fBOS model for each participant and condition is made by mirroring the right foot fBOS about the $\underline{e}_{2y}$ axis[3] and then taking average of the left and right fBOS models. The normalized version of the fBOS (Fig. 2A) is created by scaling the fBOS by foot length and width[4]. The generic fBOS model for each condition is created by averaging across all of the normalised participant fBOS models. Please refer to Appendix C for a detailed description of the method we developed to evaluate the average of a set of fBOS polygons.

2.3. Statistics

The primary outcome was the normalized fBOS area, defined as the fBOS area relative to the marker-based BOS area. The marker-based BOS area was calculated as the convex hull enclosing the area formed by the six foot markers. In addition, the fBOS length was calculated as the largest distance between points in the $\underline{e}_{2y}$ direction while the fBOS width was calculated as the largest distance between points along the $\underline{e}_{2x}$ direction (Fig. 2). Variables were calculated for and averaged over the left and right sides for each participant and condition. Note that two participants did not have a shod trial, and four participants were missing the wide stance and single stance trials.

To characterize the size of the fBOS area, we measured the normalized fBOS area for the barefoot condition with a hip-width stance (baseline condition, n=27 participants). Next, we compared the normalized fBOS area between bare and shod conditions at hip-width (n=25) to determine if footwear affects the fBOS. To quantify if stance width affected the fBOS, we compared the fBOS area when standing barefoot with feet hip-width apart to a wide stance condition (n=23). The influence of foot dominance on fBOS area was examined by comparing the fBOS area of dominant to non-dominant feet in the baseline condition (n=27). Finally, we compared the fBOS area between the single and double leg stance (baseline) conditions (n=23). When an effect was found, any differences in fBOS length and width were assessed.

[3]The fBOS of the right foot is reflected about the $\underline{e}_{2y}$ axis to make it an equivalent left foot

[4]Note that foot length and width are defined differently for the PIG and IOR marker sets. See Appendix A and Appendix B for details.

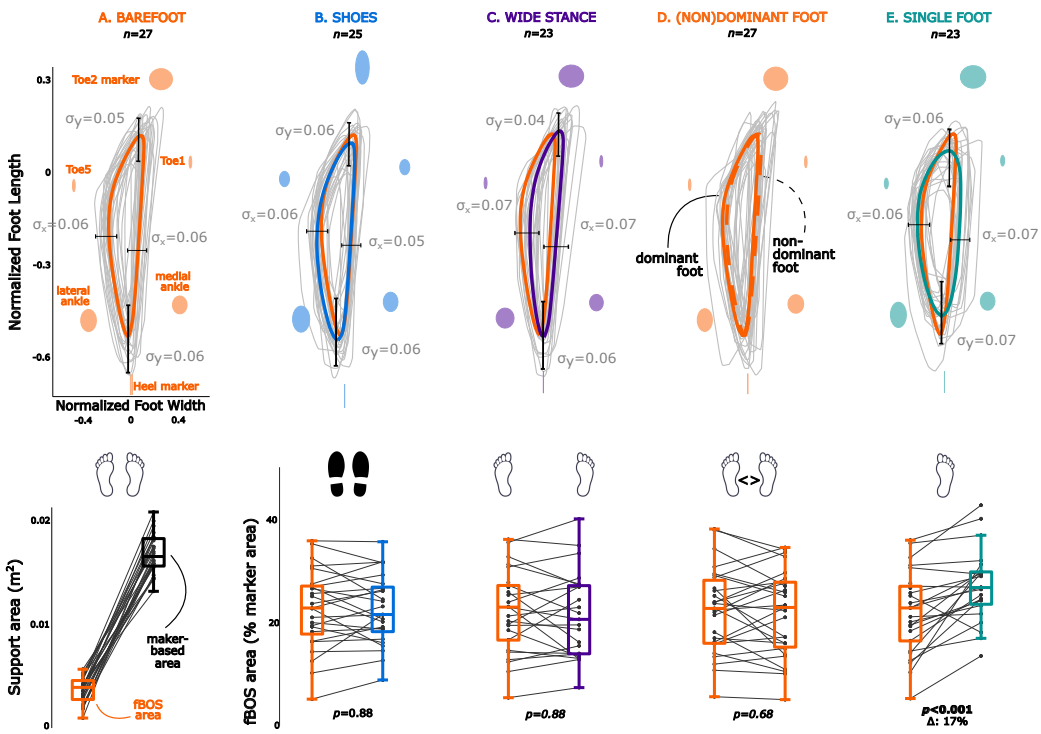

Figure 3: **Functional Base of Support (fBOS) area across conditions.** The normalized convex hull is shown for all participants (averaged over left and mirrored right side, gray lines). The average convex hull over all participants is shown in bold, coloured lines. The average (plus standard deviation) normalized locations of the foot markers are shown in colored areas. The average convex hull of the baseline condition (barefoot, two feet, hip-width apart) is plotted over the other conditions for reference. The standard deviation of the maximum front, back and side points across individual convex hulls are shown. The bottom section shows box plots (mean, interquartile range across the participants) of the absolute and relative fBOS area for the different conditions.

Conditions were compared using 2-sided Wilcoxon signed-rank tests for paired samples with significance set at $p < 0.05$. Reported results are median and interquartile values unless mentioned otherwise. Statistical analyses and all bespoke analyses above were implemented and using Matlab (version 2021a, Natick, MA, USA).

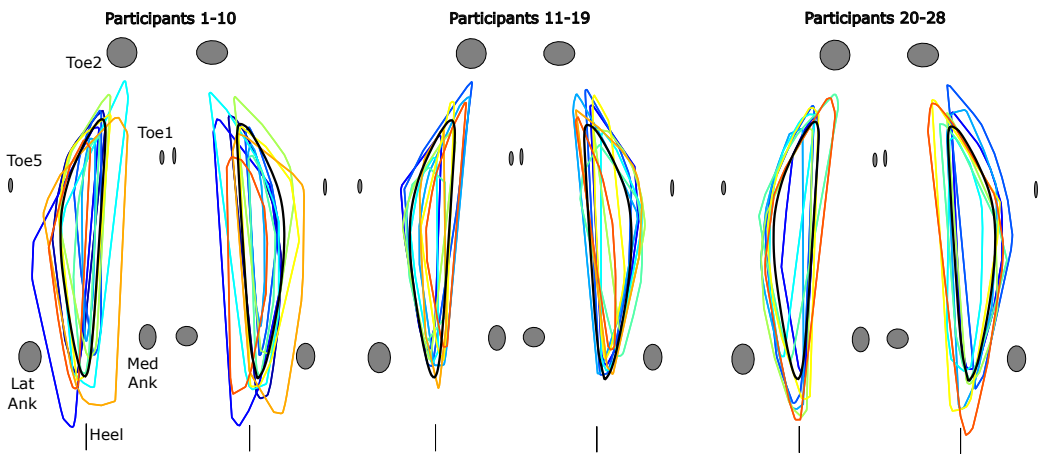

Figure 4: **Functional Base of Support (fBOS) for individual participants.** The normalized convex hull is shown for each participant (spread across three arbitrary groups for visibility) to show the variance in shape and area. The group average is shown in a thick black line. The average and standard deviations of the normalized locations of the foot markers are shown in gray.

3. Results

When barefoot, the fBOS area is 23% the size of the marker-based BOS (Fig. 3A). The barefoot fBOS is generally slightly broader in the forefoot compared to the heel, and it extends slightly beyond both the ankle and the metatarsal markers of the toe in anterior-posterior direction. There is a large variability between participants in terms of shape and area, with the normalized fBOS area ranging from 5% to 36% (Fig. 4).

The normalized fBOS area is unaffected by footwear ($p = 0.88$), stance width ($p = 0.88$), and foot dominance ($p = 0.68$) but differs between single and double stance ($p = 0.0003$). The median normalized fBOS area is 17% larger during barefoot single stance than during double-stance ($p = 0.0003$; Fig. 3): fBOS width increases by 11% (from 3.9 ± 1.5 cm to 4.3 ± 0.6 cm; $p = 0.0003$), while fBOS length decreases by 16% (from 17.6 ± 3.3 cm to 14.8 ± 3.3 cm, $p < 0.001$).

4. Discussion

The accuracy of margin-of-stability depends on both the dynamic balance model Hof (2008); Kajita and Tani (1991); Millard et al. (2012) and the BOS

model Sloot et al. (2020). Unfortunately, there is no standard definition of the BOS Watson et al. (2021), which is most often approximated using one or two motion capture markers or the COP. In this work, we have sought to measure and study the size of fBOS across a range of everyday conditions, to improve the accuracy of the margin-of-stability specifically and balance analysis in general.

While the fBOS is an improvement over existing BOS models Watson et al. (2021), our study has several limitations. The task that we have used to measure the fBOS necessarily can only be applied to postures in which someone can stand stably. As such, it is unclear how the fBOS changes during dynamic movements in which a step must be taken. In addition, the task we have used to measure the fBOS is inherently dependent on a variety of factors: balance, strength, coordination, and motivation. As such, we cannot exclude the possibility that the measured areas have been affected by motivation or instructions, particularly given the large variability between the young, able-bodied participants. This can also be indicative of a difference in balance ability, but we could not analyze this because we did not perform balance tests.

In addition, there are limitations related specifically to our experiments. We did not control for the type of shoe nor the stiffness of the foot. Variation in shoe type may affect our results by introducing variability in support and also in how each shoe affects the mechanoreceptors of the foot. Participants with stiffer feet (typically with high arches) may be able to produce larger fBOS areas than participants with more flexible feet. In addition, foot dominance was self-reported, and several people had difficulty indicating their dominant leg. Finally, we did not have a uniformly complete dataset and some trials had to be manually removed. Of the data that we collected, two participants did not have a shod trial and four participants were missing the wide stance and single stance trials. We did not include in our population the data of one participant whose FM2 marker was incorrectly placed, another participant with force data problems, and a final participant with abnormally large fBOS areas. The participant with abnormally large fBOS areas was able to raise parts of their feet and still meet the criteria that $\mathrm{M}\sin\psi_X \leq 1.5\,\mathrm{cm}$ and $\mathrm{W}\sin\theta_Y \leq 1.5\mathrm{cm}$ as described in Sec. 2.1. While using a single threshold as described in Sec. 2.1 is convenient, it is likely that a single threshold is not appropriate for all participants. Our criteria for ensuring that the foot is flat on the floor might be improved by measuring a subject-specific threshold or by using pressure mats that can directly

measure if the footprint area has changed.

Despite these limitations, our main finding is similar to existing literature: the fBOS is considerably smaller in size than a marker-based BOS. Our results show that the fBOS is 23% the size of a marker-based BOS, which is less than the 60% reported for persons under the age of 60 King et al. (1994), less than the 47% reported for persons aged 20 to 23 years Tomita et al. (2021), but larger than the effective base-of-support (eBOS) of Hof and Curtze Hof and Curtze (2016). Some of these differences might be due to the different methods used to define the size of the BOS: King et al. King et al. (1994) restricted their study to examine just the anterior-posterior direction, Tomita et al. Tomita et al. (2021) considered the total support area enclosed by both feet, while we considered the area under each foot separately. In contrast, Hof and Curtze's Hof and Curtze (2016) eBOS has been reduced in size to account for neural and mechanical delays involved in correcting standing balance after unexpected perturbations.

While our results agree with the literature King et al. (1994); Tomita et al. (2021); Hof and Curtze (2016) that the fBOS is smaller than the BOS, we have extended the literature both with a richer geometric model of the fBOS and a systematic study of how four everyday conditions affect the fBOS. The polygon model of the fBOS that we have developed is able to capture details about the shape of the fBOS that are not apparent when the fBOS is measured in one King et al. (1994), or a series of directions Tomita et al. (2021). In addition, our work also shows that the fBOS is unaffected by footwear, stance width, and foot dominance but is slightly larger in single versus double stance. It is presently unclear if the fBOS is larger during single stance due to the increased load or because of an artifact of the task: during double stance it is much easier to transfer weight to the other foot rather than use the medial side of the foot to support the COP. If this interpretation is correct, than the medial side of the fBOS is not completely assessed during double stance.

When used in combination with a dynamic balance model Hof (2008); Kajita and Tani (1991); Millard et al. (2012), the fBOS makes it possible to calculate the margin-of-stability more accurately. The fBOS can improve the accuracy of the margin-of-stability calculation in both the anterior-posterior direction (16% of foot length at the heel, and 17% at the toe), and the mediolateral direction (23% of the total foot width at the toe metatarsal marker and 12% at the ankle). In physical terms, the fBOS model can improve the accuracy of the BOS and therefore the margin-of-stability by

4.7cm at the heel, 5.0cm at the toe, and 2.3cm at the sides of the forefoot for an average-sized 30cm by 10cm foot. In the context of balance analysis, these differences are large and can mean the difference between standing stably and having to take a step. As previous studies show that the fBOS declines with ageing King et al. (1994); Tomita et al. (2021), we next plan to evaluate and model the fBOS in older persons and patient populations.

5. Conclusion

The fBOS can improve the accuracy of dynamic balance analysis in general and the margin of stability specifically. A single fBOS model can be used in many different scenarios since the fBOS area is unaffected by footwear, stance-width, and foot dominance. A modest additional improvement in accuracy can be realized by using separate fBOS models for single and double stance. The presented model offers a generally applicable definition for the fBOS, which can be applied to foot marker data captured during walking or other movements.

Conflict of Interest Statement

The authors declare that the research was conducted in the absence of any commercial or financial relationships that could be construed as a potential conflict of interest.

Author Contributions

LHS and MM designed the experiment; LHS was responsible for participant recruitment, data collection and data processing; MM created the fBOS model and basic code; LHS ran the statistics; LHS and MM analyzed and interpreted the data; LHS and MM wrote the manuscript, and generated the figures.

Funding

The results presented here have been obtained as part of the project "HEIAGE" (P2017-01-00), which is funded by the CarlZeiss-Foundation (Germany). LHS is supported by The Rosetrees / Stoneygate Trusts Newcastle University Fellowship. MM gratefully acknowledges financial support from

the Deutsche Forschungsgemeinschaft (DFG, German Research Foundation) under Germany's Excellence Strategy (EXC 2075 – 390740016) through the Stuttgart Center for Simulation Science (SimTech), and from DFG project number 540349998.

Acknowledgements

The authors like to thank Elif Öztürk, Klaus Breuer, Lukas Becker, Qiao Chen, Maedeh Taeb, Joel Grathwohl, and Thomas Gerhardy for their help with data collection and processing. We also like to thank Katja Mombaur for the funding through the HeiAGE project.

Data and Code Availability Statement

The outcome variables for all individuals that are used for statistical analysis are made available in the supplementary material file: 'SupMat_individuals_datavalues_v3.xls'. The raw data files are available from the corresponding authors on reasonable request. The functions to calculate the fBOS model, to average fBOS convex hulls and to calculate fBOS models for the IORadj and PIG marker models, as well as example data to use these functions, are shared at GitHub: https://github.com/mjhmilla/functionalBaseOfSupport.

References

Cappozzo, A., Catani, F., Della Croce, U., Leardini, A., 1995. Position and orientation in space of bones during movement: anatomical frame definition and determination. Clinical Biomechanics 10, 171–178. doi:10.1016/0268-0033(95)91394-T.

Cavanagh, P.R., 1999. Plantar soft tissue thickness during ground contact in walking. Journal of Biomechanics 32, 623 – 628. doi:10.1016/S0021-9290(99)00028-7.

Davis III, R.B., Ounpuu, S., Tyburski, D., Gage, J.R., 1991. A gait analysis data collection and reduction technique. Human movement science 10, 575–587. doi:10.1016/0167-9457(91)90046-Z.

Gefen, A., Megido-Ravid, M., Itzchak, Y., 2001. In vivo biomechanical behavior of the human heel pad during the stance phase of gait. Journal of Biomechanics 34, 1661 – 1665. doi:10.1016/S0021-9290(01)00143-9.

Grood, E.S., Suntay, W.J., 1983. A Joint Coordinate System for the Clinical Description of Three-Dimensional Motions: Application to the Knee. Journal of Biomechanical Engineering 105, 136–144. doi:10.1115/1.3138397.

Hof, A.L., 2008. The 'extrapolated center of mass' concept suggests a simple control of balance in walking. Human Movement Science 27, 112–125. doi:10.1016/j.humov.2007.08.003.

Hof, A.L., Curtze, C., 2016. A stricter condition for standing balance after unexpected perturbations. Journal of biomechanics 49, 580–585. doi:10.1016/j.jbiomech.2016.01.021.

Kajita, S., Tani, K., 1991. Study of dynamic biped locomotion on rugged terrain-derivation and application of the linear inverted pendulum mode, in: Proceedings of the 1991 IEEE International Conference on Robotics and Automation, pp. 1405–1411. doi:10.1109/ROBOT.1991.131811.

King, M.B., Judge, J.O., Wolfson, L., 1994. Functional base of support decreases with age. Journal of gerontology 49, M258–M263. doi:10.1093/geronj/49.6.M258.

Leardini, A., Biagi, F., Merlo, A., Belvedere, C., Benedetti, M.G., 2011. Multi-segment trunk kinematics during locomotion and elementary exercises. Clinical Biomechanics 26, 562–571. doi:10.1016/j.clinbiomech.2011.01.015.

Leardini, A., Sawacha, Z., Paolini, G., Ingrosso, S., Nativo, R., Benedetti, M.G., 2007. A new anatomically based protocol for gait analysis in children. Gait & posture 26, 560–571. doi:10.1016/j.gaitpost.2006.12.018.

Melzer, I., Benjuya, N., Kaplanski, J., 2004. Postural stability in the elderly: a comparison between fallers and non-fallers. Age and ageing 33, 602–607. doi:10.1093/ageing/afh218.

Millard, M., McPhee, J., Kubica, E., 2012. Foot Placement and Balance in 3D. Journal of Computational and Nonlinear Dynamics 7. doi:10.1115/1.4005462.

Sloot, L.H., Millard, M., Werner, C., Mombaur, K., 2020. Slow but steady: Similar sit-to-stand balance at seat-off in older vs. younger adults. Frontiers in Sports and Active Living 2. doi:10.3389/fspor.2020.548174.

Tomita, H., Kuno, S., Kawaguchi, D., Nojima, O., 2021. Limits of stability and functional base of support while standing in community-dwelling older adults. Journal of Motor Behavior 53, 83–91. doi:10.1080/00222895.2020.1723484.

Vicon®, 2002. Plug-in-gait modelling instructions.

Watson, F., Fino, P.C., Thornton, M., Heracleous, C., Loureiro, R., Leong, J.J.H., 2021. Use of the margin of stability to quantify stability in pathologic gait – a qualitative systematic review. BMC Musculoskeletal Disorders 22, 597. doi:10.1186/s12891-021-04466-4.

Appendix A. Constructing the fBOS foot frame from adjusted Istituti Ortopedici Rizzoli (IORadj) data

We begin by defining a notation convention for vectors, unit vectors, rotation matrices, and frames using a combination of super and subscripts so that we can be specific about each kinematic quantity. For example, the vector ${}^{1}_{\mathrm{A}}\underline{r}_{\mathrm{B}}$ originates from point A, goes to point B and is resolved in the coordinates of $\mathcal{K}_1$ (${}^{\mathrm{coord}}_{\mathrm{from}}\underline{r}_{\mathrm{to}}$). To reduce the number of super and subscripts we will omit writing '0' for $\mathcal{K}_0$ (for example writing $\underline{r}_1$ instead of ${}^{0}_{0}\underline{r}_1$) unless we are trying to be very explicit. Unit vectors require a label for the unit vector and the coordinates that it is described in: ${}^{0}\underline{e}_{1\mathrm{x}}$ is the x-axis unit vector of $\mathcal{K}_1$ resolved in the coordinates of $\mathcal{K}_0$. Similarly, the notation for rotation matrices indicates the origin and destination frames (${}^{\mathrm{to}}\underline{\underline{R}}_{\mathrm{from}}$): ${}^{1}\underline{\underline{R}}_{0}$ transforms vectors from $\mathcal{K}_0$ to $\mathcal{K}_1$ (and $({}^{1}\underline{\underline{R}}_{0})^{\mathrm{T}}$ from $\mathcal{K}_1$ to $\mathcal{K}_0$). A frame is defined by a vector that points to its origin and a rotation matrix that defines its orientation with respect to another frame: $\mathcal{K}_1$ has an origin ${}^{0}_{0}\underline{r}_1$ and orientation ${}^{0}\underline{\underline{R}}_{1}$ relative to $\mathcal{K}_0$. Using this convention we can precisely describe how the foot-fixed frames $\mathcal{K}_1$ and $\mathcal{K}_2$ are formed using the locations of optical markers on the foot and a quiet standing trial.

The origin of the foot-fixed axis $\mathcal{K}_1$ (Fig. 2B, left) as being halfway between the two ankle markers

$$ {}^{0}\underline{r}_1 = \frac{1}{2}\left({}^{0}\underline{r}_{\mathrm{FAL}} + {}^{0}\underline{r}_{\mathrm{TAM}}\right). \tag{A.1} $$

Averaging both ankle markers should reduce small recording errors and puts the origin below the ankle joint which makes the fBOS a bit more intuitive to interpret. Next, the long-axis of the foot is formed using the markers

$$ {}^{0}\underline{r}_{\mathrm{y}} = \frac{1}{2}\left({}^{0}\underline{r}_{\mathrm{FM5}} + {}^{0}\underline{r}_{\mathrm{FM1}}\right) - {}^{0}\underline{r}_{\mathrm{FCC}} \tag{A.2} $$

on the forefoot and heel. Averaging over both forefoot markers should also reduce small recording errors. It should be noted that the FM2 marker in this study was placed on the tip of the longest toe (Fig. 2B). We avoided using the FM2 marker when defining $\mathcal{K}_1$ because this marker can move relative to the foot (as the toes flex) and also because it is not placed at a consistent anatomical location: either the first or the second toe can be the longest toe. Once normalized by the Euclidean norm the vector

$$ {}^{0}\underline{e}_{1\mathrm{y}} = \frac{{}^{0}\underline{r}_{\mathrm{y}}}{|{}^{0}\underline{r}_{\mathrm{y}}|}. \tag{A.3} $$

forms the y-axis of $\mathcal{K}_1$. The transverse axis of the left foot is given by

$$ {}^{0}\underline{r}_{\mathrm{x}} = {}^{0}\underline{r}_{\mathrm{FM1}} - {}^{0}\underline{r}_{\mathrm{FM5}}. \tag{A.4} $$

The transverse axis of the right foot is

$$ {}^{0}\underline{r}_{\mathrm{x}}^{\mathrm{R}} = {}^{0}\underline{r}_{\mathrm{FM5}} - {}^{0}\underline{r}_{\mathrm{FM1}} \tag{A.5} $$

defined using the opposite direction to preserve the orientation of the final $\underline{e}_{2\mathrm{z}}$ axis. After subtracting any components in ${}^{0}\underline{e}_{1\mathrm{y}}$

$$ {}^{0}\underline{r}_{\mathrm{x}'} = {}^{0}\underline{r}_{\mathrm{x}} - \left({}^{0}\underline{r}_{\mathrm{x}} \cdot {}^{0}\underline{e}_{1\mathrm{y}}\right) {}^{0}\underline{e}_{1\mathrm{y}} \tag{A.6} $$

we can form

$$ {}^{0}\underline{e}_{1\mathrm{x}} = \frac{{}^{0}\underline{r}_{\mathrm{x}'}}{|{}^{0}\underline{r}_{\mathrm{x}'}|} \tag{A.7} $$

the x-axis. The z-axis is given by

$$ {}^{0}\underline{e}_{1\mathrm{z}} = {}^{0}\underline{e}_{1\mathrm{x}} \times {}^{0}\underline{e}_{1\mathrm{y}}. \tag{A.8} $$

and together these direction vectors form the rotation matrix (Fig. 2B, left)

$$ {}^{0}\underline{\underline{R}}_{1} = \left[{}^{0}\underline{e}_{1\mathrm{x}},\, {}^{0}\underline{e}_{1\mathrm{y}},\, {}^{0}\underline{e}_{1\mathrm{z}}\right]. \tag{A.9} $$

Finally, using the constant offset vector ${}^{1}_{1}\underline{r}_{2}$ and rotation matrix ${}^{1}\underline{\underline{R}}_{2}$ we transform the orientation of $\mathcal{K}_1$ to $\mathcal{K}_2$

$$ {}^{0}\underline{\underline{R}}_{2} = {}^{0}\underline{\underline{R}}_{1}\, {}^{1}\underline{\underline{R}}_{2} \tag{A.10} $$

such that the z-axis is normal to the foot print and the origin

$$ {}^{0}\underline{r}_{2} = {}^{0}\underline{r}_{1} + {}^{0}\underline{\underline{R}}_{2}\, {}^{2}_{1}\underline{r}_{2} \tag{A.11} $$

lies within the foot print (Fig. 2B, right). We can now locate the j fBOS points

$$ {}^{0}_{0}\underline{r}_{\mathrm{f}}^{j} = {}^{0}_{0}\,\underline{r}_{2} + {}^{0}\underline{\underline{R}}_{2} \begin{pmatrix} {}^{2}_{2}x^{j}\,\mathrm{W} \\ {}^{2}_{2}y^{j}\,\mathrm{L} \\ 0 \end{pmatrix} \tag{A.12} $$

in the lab frame $\mathcal{K}_0$ where

$$ \mathrm{W} = \frac{1}{2}\left|(\underline{r}_{\mathrm{FM5}} - \underline{r}_{\mathrm{FM1}}) \cdot \underline{e}_{2\mathrm{x}}\right| + \frac{1}{2}\left|(\underline{r}_{\mathrm{TAM}} - \underline{r}_{\mathrm{FAL}}) \cdot \underline{e}_{2\mathrm{x}}\right| \tag{A.13} $$

is the width of the foot,

$$\mathrm{L} = (\underline{r}_{\mathrm{FM2}} - \underline{r}_{\mathrm{FCC}}) \cdot \underline{e}_{2\mathrm{y}} \tag{A.14}$$

is the length of the foot, and

$$\mathrm{M} = \left(\frac{1}{2} (\underline{r}_{\mathrm{FM1}} + \underline{r}_{\mathrm{FM5}}) - \frac{1}{2} (\underline{r}_{\mathrm{FAL}} + \underline{r}_{\mathrm{TAM}}) \right) \cdot \underline{e}_{2\mathrm{y}} \tag{A.15}$$

is the length of the participant's mid-foot. With the coordinates of the fBOS model in $\mathcal{K}_0$ the fBOS model can be used to interpret other data such as the margin-of-stability.

The offset vector ${}^{2}_{1}\underline{r}_2$ and rotation matrix ${}^{1}\underline{\underline{R}}_2$ needed to transform $\mathcal{K}_1$ to $\mathcal{K}_2$ are evaluated using the data from a quiet standing trial when the foot can be considered to be flat on the ground. During quiet standing we evaluate ${}^{0}\underline{e}_{2\mathrm{y}}$ by projecting ${}^{0}\underline{e}_{1\mathrm{y}}$ onto the ground

$${}^{0}\underline{r}_{2\mathrm{y}} = {}^{0}\underline{e}_{1\mathrm{y}} - \left({}^{0}\underline{e}_{1\mathrm{y}} \cdot {}^{0}\underline{e}_{0\mathrm{z}}\right) {}^{0}\underline{e}_{0\mathrm{z}} \tag{A.16}$$

and then by normalizing the result to yield

$${}^{0}\underline{e}_{2\mathrm{y}} = \frac{{}^{0}\underline{r}_{2\mathrm{y}}}{|{}^{0}\underline{r}_{2\mathrm{y}}|}. \tag{A.17}$$

Similarly, we project ${}^{0}\underline{e}_{1\mathrm{x}}$ onto the ground

$${}^{0}\underline{r}_{2\mathrm{x}} = {}^{0}\underline{e}_{1\mathrm{x}} - \left({}^{0}\underline{e}_{1\mathrm{x}} \cdot {}^{0}\underline{e}_{0\mathrm{z}}\right) {}^{0}\underline{e}_{0\mathrm{z}} \tag{A.18}$$

remove any components in ${}^{0}\underline{e}_{2\mathrm{y}}$

$${}^{0}\underline{r}_{2\mathrm{x}'} = {}^{0}\underline{r}_{2\mathrm{x}} - \left({}^{0}\underline{r}_{2\mathrm{x}} \cdot {}^{0}\underline{e}_{2\mathrm{y}}\right) {}^{0}\underline{e}_{2\mathrm{y}} \tag{A.19}$$

and normalize the result

$${}^{0}\underline{e}_{2\mathrm{x}} = \frac{{}^{0}\underline{r}_{2\mathrm{x}'}}{|{}^{0}\underline{r}_{2\mathrm{x}'}|}. \tag{A.20}$$

to form the x-axis of $\mathcal{K}_2$. The z-axis of $\mathcal{K}_2$ is found using the cross product

$${}^{0}\underline{e}_{2\mathrm{z}} = {}^{0}\underline{e}_{2\mathrm{x}} \times {}^{0}\underline{e}_{2\mathrm{y}}. \tag{A.21}$$

We can now form

$${}^{0}\underline{\underline{R}}_2 = \left[{}^{0}\underline{e}_{2\mathrm{x}},\ {}^{0}\underline{e}_{2\mathrm{y}},\ {}^{0}\underline{e}_{2\mathrm{z}}\right] \tag{A.22}$$

by putting the direction vectors ${}^{0}\underline{e}_{2\mathrm{x}}$,${}^{0}\underline{e}_{2\mathrm{y}}$, and ${}^{0}\underline{e}_{2\mathrm{z}}$ into columns. Finally, we can evaluate

$$ {}^{1}\underline{\underline{R}}_{2} = \left({}^{0}\underline{\underline{R}}_{1}\right)^{\mathrm{T}} \left({}^{0}\underline{\underline{R}}_{2}\right) \tag{A.23} $$

where ${}^{\mathrm{T}}$ is the transpose operator. During quiet standing the origin of $\mathcal{K}_2$ is given by (Fig. 2B, right)

$$ {}^{0}\underline{r}_{2} = {}^{0}\underline{r}_{1} - \left({}^{0}\underline{r}_{1} \cdot {}^{0}\underline{e}_{\mathrm{z}0}\right) {}^{0}\underline{e}_{\mathrm{z}0}. \tag{A.24} $$

The offset vector between $\mathcal{K}_1$ and $\mathcal{K}_2$ is given by

$$ {}^{2}_{1}\underline{r}_{2} = \left({}^{0}\underline{\underline{R}}_{2}\right)^{\mathrm{T}} \left({}^{0}\underline{r}_{2} - {}^{0}\underline{r}_{1}\right). \tag{A.25} $$

One advantage of the IOR marker set is that there are more than the minimum of three markers on the rigid part of the foot. This redundancy makes it possible to use an alternative set of markers to evaluate the location of $\mathcal{K}_2$ than the one proposed above. For example, many of the experimental recordings in this study had gaps in the medial ankle markers due to occlusion. Rather than having to rely on interpolated values for these marker positions we instead re-defined the markers that we used to evaluate $\mathcal{K}_1$ and make a corresponding update to the offset position vector and rotation matrix to locate $\mathcal{K}_2$. For the sake of clarity we will refer to the alternative $\mathcal{K}_1$ as $\mathcal{K}_3$ and $\mathcal{K}_2$ as $\mathcal{K}_4$.

The origin of $\mathcal{K}_3$ was placed between the two metatarsal markers

$$ {}^{0}\underline{r}_{3} = \frac{1}{2}\left({}^{0}\underline{r}_{\mathrm{FM1}} + {}^{0}\underline{r}_{\mathrm{FM5}}\right) \tag{A.26} $$

with vector

$$ {}^{0}\underline{r}_{3\mathrm{y}} = \frac{1}{2}\left({}^{0}\underline{r}_{\mathrm{FM5}} + {}^{0}\underline{r}_{\mathrm{FM1}}\right) - {}^{0}\underline{r}_{\mathrm{FCC}} \tag{A.27} $$

that forms the y-axis

$$ \underline{e}_{3\mathrm{y}} = \frac{{}^{0}\underline{r}_{3\mathrm{y}}}{|{}^{0}\underline{r}_{3\mathrm{y}}|} \tag{A.28} $$

pointing from the heel to ${}^{0}\underline{r}_{3}$. The vector that forms the x-axis went from the FM5 marker to the FM1 marker (the opposite for the right foot)

$$ {}^{0}\underline{r}_{3\mathrm{x}} = {}^{0}\underline{r}_{\mathrm{FM1}} - {}^{0}\underline{r}_{\mathrm{FM5}}, \tag{A.29} $$

had components in the y-axis removed

$$ {}^{0}\underline{r}_{3\mathrm{x}'} = {}^{0}\underline{r}_{3\mathrm{x}} - \left({}^{0}\underline{r}_{3\mathrm{x}} \cdot \underline{e}_{3\mathrm{y}}\right) \underline{e}_{3\mathrm{y}}, \tag{A.30} $$

and finally was normalized

$$ {}^{0}\underline{e}_{3\mathrm{x}} = \frac{{}^{0}\underline{r}_{\mathrm{b}}}{|{}^{0}\underline{r}_{\mathrm{b}}|}. \tag{A.31} $$

As before, the z-axis is given by the cross product

$$ {}^{0}\underline{e}_{3\mathrm{z}} = {}^{0}\underline{e}_{3\mathrm{x}} \times {}^{0}\underline{e}_{3\mathrm{y}} \tag{A.32} $$

of the x and y direction vectors. Concatenating these direction vectors in a matrix

$$ {}^{0}\underline{\underline{R}}_{3} = \left[{}^{0}\underline{e}_{3\mathrm{x}}, {}^{0}\underline{e}_{3\mathrm{y}}, {}^{0}\underline{e}_{3\mathrm{z}}\right] \tag{A.33} $$

forms the rotation matrix from $\mathcal{K}_3$ to $\mathcal{K}_0$. By making use of a quiet standing trial and Eqns. A.16-A.25 the offset position vector and rotation matrix were calculated to put the origin of $\mathcal{K}_4$ on the foot print and to align the ${}^{0}\underline{e}_{4\mathrm{x}} - {}^{0}\underline{e}_{4\mathrm{y}}$ plane with the foot print.

Since the fBOS is defined with respect to $\mathcal{K}_2$ we also updated the coordinates of the fBOS to be located with respect to $\mathcal{K}_4$. Using a quiet standing trial that include a clean recording of all of the foot markers we calculated the locations of each of the $j = 1 \ldots \mathrm{M}$ fBOS points

$$ {}^{0}_{0}\underline{r}^{j}_{\mathrm{f}} = {}^{0}_{0}\underline{r}_{2} + {}^{0}\underline{\underline{R}}_{2} \begin{pmatrix} {}^{2}_{2}x^{j}\,\mathrm{W} \\ {}^{2}_{2}y^{j}\,\mathrm{L} \\ 0 \end{pmatrix}. \tag{A.34} $$

for a specific participant in the lab frame ($\mathcal{K}_0$). With the fBOS points resolved in $\mathcal{K}_0$, we could now resolve these points in $\mathcal{K}_4$

$$ {}^{4}_{4}\underline{r}^{j}_{\mathrm{f}} = \left({}^{0}\underline{\underline{R}}_{4}\right)^{\mathrm{T}} \left({}^{0}_{0}\underline{r}^{j}_{\mathrm{f}} - {}^{0}_{0}\underline{r}_{4}\right). \tag{A.35} $$

The resulting $j = 1 \ldots \mathrm{M}$ fBOS points can now be evaluated for any foot posture without requiring the ankle markers using

$$ {}^{0}_{0}\underline{r}^{j}_{\mathrm{f}} = {}^{0}_{0}\underline{r}_{3} + {}^{0}\underline{\underline{R}}_{3} \left({}^{3}_{3}\underline{r}_{4} + {}^{3}\underline{\underline{R}}_{4}\, {}^{4}_{4}\underline{r}^{j}_{\mathrm{f}}\right). \tag{A.36} $$

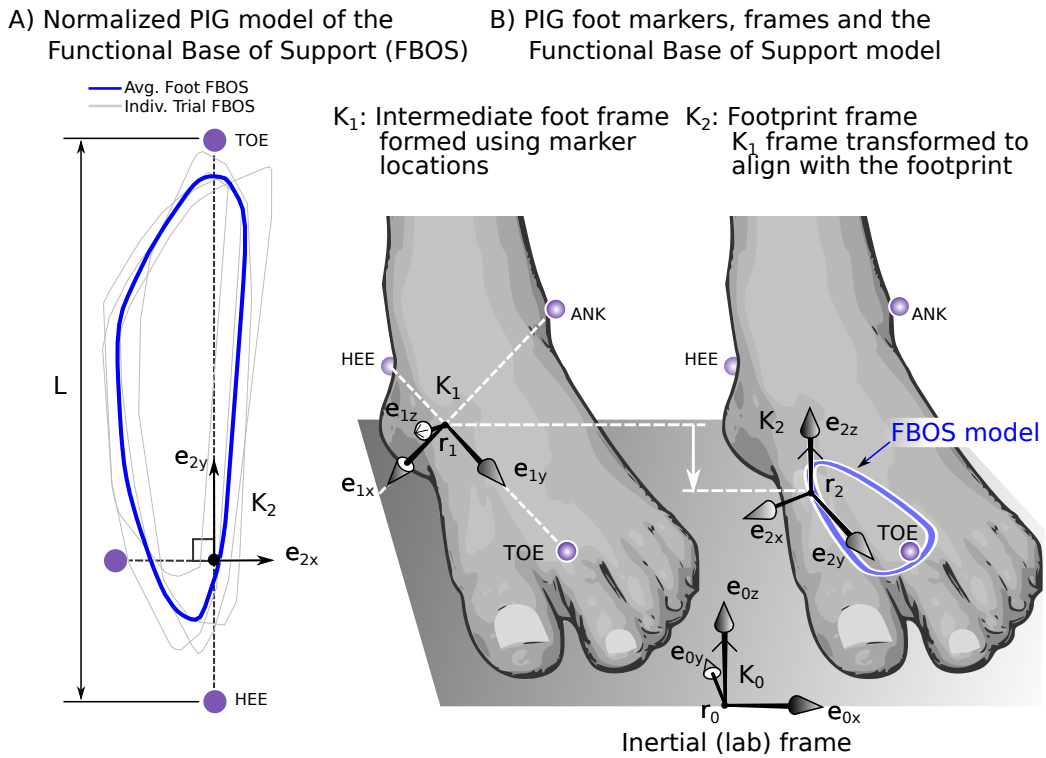

Figure B.5: The fBOS polygon (A) is located in the $\mathcal{K}_2$ that has been constructed such the $\underline{e}_{2x} - \underline{e}_{2y}$ is in the plane of the footprint, the origin lies between the heel and toe markers. The $\mathcal{K}_2$ is located by first forming the $\mathcal{K}_1$ using the positions of the markers on the foot (B, left). Next, using a quiet standing trial the offset vector and rotation matrix are be calculated to transform $\mathcal{K}_1$ to $\mathcal{K}_2$. As with the IOR data set, once the offset vector and rotation matrix have been evaluated the $\mathcal{K}_2$ can be located with the foot in any posture.

Appendix B. Constructing the fBOS foot frame from Plug-in-gait (PIG) data

The fBOS model can be applied to other marker sets as long as the following conditions are met: there are at least 3 markers on the foot (excluding the toes), the markers are not aligned, nor in the same location. Conversions to new marker sets can be made by modifying the equations that calculate the foot and offset frames and by collecting a static trial includes both the new marker set and the IOR/PIG marker set. The static trial that includes

both marker sets is needed to resolve the normalised fBOS model in the foot frame of the new marker set. As such, the presented model can improve the margin of stability estimations in past and in future studies that use either the IOR/PIG marker sets and can be expanded to other marker models provided the necessary static trial is available. In this appendix, we demonstrate the procedure of how to apply an fBOS model from an IOR marker set to a PIG marker set, as this procedure is going to be similar for any other marker set.

The foot-fixed frame for a PIG marker set is constructed using a comparable approach to the one used in Appendix A. The long axis of the foot is defined using

$$ {}^{0}\underline{r}_{\mathrm{y}} = {}^{0}\underline{r}_{\mathrm{TOE}} - {}^{0}\underline{r}_{\mathrm{HEE}}. \tag{B.1} $$

which becomes

$$ {}^{0}\underline{e}_{1\mathrm{y}} = \frac{\underline{r}_{\mathrm{y}}}{|\underline{r}_{\mathrm{y}}|} \tag{B.2} $$

after normalization. Next we evaluate

$$ {}_{\mathrm{ANK}}\underline{r}_{\mathrm{HEE}} = {}_{0}\underline{r}_{\mathrm{HEE}} - {}_{0}\underline{r}_{\mathrm{ANK}} \tag{B.3} $$

and remove components in ${}^{0}\underline{e}_{1\mathrm{y}}$ to yield

$$ \underline{r}_{1\mathrm{x}} = {}_{\mathrm{ANK}}\,\underline{r}_{\mathrm{HEE}} - \left({}_{\mathrm{ANK}}\underline{r}_{\mathrm{HEE}} \cdot {}^{0}\underline{e}_{1\mathrm{y}}\right) {}^{0}\underline{e}_{1\mathrm{y}} \tag{B.4} $$

the transverse vector of the foot. After normalization

$$ \underline{e}_{1\mathrm{x}} = \frac{\underline{r}_{1\mathrm{x}}}{|\underline{r}_{1\mathrm{x}}|} \tag{B.5} $$

we are left with the x-axis of $\mathcal{K}_1$. The z-axis is formed using the cross-product

$$ \underline{e}_{1\mathrm{z}} = \underline{e}_{1\mathrm{x}} \times \underline{e}_{1\mathrm{y}} \tag{B.6} $$

which allows us to form

$$ {}^{0}\underline{\underline{R}}_{1} = \left[\underline{e}_{1\mathrm{x}},\, \underline{e}_{1\mathrm{y}},\, \underline{e}_{1\mathrm{z}}\right]. \tag{B.7} $$

Using the rotation matrix ${}^{1}\underline{\underline{R}}_{2}$ and vector ${}^{2}_{1}\underline{r}_{2}$ from the quiet standing trial (formulated using the same method described in Appendix A) we can evaluate the orientation of $\mathcal{K}_2$

$$ {}^{0}\underline{\underline{R}}_{2} = {}^{0}\underline{\underline{R}}_{1}\,{}^{1}\underline{\underline{R}}_{2} \tag{B.8} $$

and its location

$$ {}^{0}\underline{r}_2 = {}^{0}\underline{r}_1 + \left({}^{0}\underline{\underline{R}}_2\right) {}^{2}_{1}\underline{r}_2. \tag{B.9} $$

The frame $\mathcal{K}_2$ can be thought of as the footprint frame since it is formed to be coincident with the footprint during the quiet standing trial. As with the IOR model, the $j = 1 \ldots \mathrm{M}$ points of the PIG fBOS model

$$ {}^{0}_{0}\underline{r}^{j}_{\mathrm{f}} = {}^{0}_{0}\,\underline{r}_2 + {}^{0}\underline{\underline{R}}_2 \begin{pmatrix} {}^{2}_{2}x^{j}\,\mathrm{L} \\ {}^{2}_{2}y^{j}\,\mathrm{L} \\ 0 \end{pmatrix} \tag{B.10} $$

once resolved in the $\mathcal{K}_0$ can be used for subsequent analysis.

The term L in Eqn. B.10 is the length

$$ \mathrm{L} = (\underline{r}_{\mathrm{TOE}} - \underline{r}_{\mathrm{HEE}}) \cdot \underline{e}_{2\mathrm{y}}. \tag{B.11} $$

of the foot given for the PIG fBOS model. Since both the length, mid-foot length, and width of the PIG fBOS model are normalized by length, this fBOS model will not closely fit participant's who happen to have feet that are narrower or wider than the feet that were used to construct the fBOS model. We have normalized the PIG fBOS model only by length because the PIG marker layout does not make it possible to estimate foot width from the marker locations alone. The IOR fBOS model, in contrast, has enough markers to permit scaling the model by both length and width and as a result will fit participants with narrower or wider feet more closely than the PIG fBOS model.

Appendix C. A method to average fBOS polygons

Due to the variety of shapes and sizes of individual fBOS areas we had to develop a method to compute the average fBOS across all N participants. First, each foot is registered to a common point. Fortunately, each individual fBOS trial in the dataset has a distinct posterior point that aligns with the heel. We ordered participant i's fBOS data to begin with the heel point and to proceed counter-clock-wise around the foot resulting in an array of points where the coordinates of the jth point is given by (x_i^j, y_i^j) and the entire array of $j = 1 \ldots \mathrm{M}_i$ points of participant i are given by $(\underline{\mathrm{x}}_i, \underline{\mathrm{y}}_i)$ (Fig. C.6). Second, we evaluated the cumulative arc-length[5] of $(\underline{\mathrm{x}}_i, \underline{\mathrm{y}}_i)$ and normalized

[5]The cumulative sum of the distance between adjacent pairs of points on the curve.

it to begin from 0 (heel) and end at 1 (back to heel after circling the foot) to form the vector $\underline{s}_i$ (indicated in Fig. C.6 A, B, and C as s). By linearly interpolating $(\underline{x}_i, \underline{y}_i)$ with $\underline{s}_i$ we can use s to identify equivalent points [6] across each participant's fBOS. To evaluate the average set of points $(\underline{x}, \underline{y})$ from $(\underline{x}_i, \underline{y}_i)$ across all N participants we evaluate

$$\underline{x}(s) = \frac{1}{\mathrm{N}} \sum_{i=1}^{\mathrm{N}} \underline{x}_i(s) \tag{C.1}$$

and

$$\underline{y}(s) = \frac{1}{\mathrm{N}} \sum_{i=1}^{\mathrm{N}} \underline{y}_i(s) \tag{C.2}$$

across a series of values of s from 0 to 1. To ensure that every node in each individual fBOS is evaluated in Eqns. C.1 and C.2, we form $\underline{s}$: the sorted vector of unique values in the set $[\underline{s}_1 \cup \underline{s}_2 \ldots \cup \underline{s}_{\mathrm{N}}]$ of all N participants (Fig. C.6 contains an example where two fBOS models are averaged). Finally, the convex hull of the resulting average $(\underline{x}, \underline{y})$ is taken to reduce the number of points needed to describe the fBOS polygon.

[6] For example, $s = 0$ corresponds to the heel for every participant while $s = 0.5$ will be close to the toe.

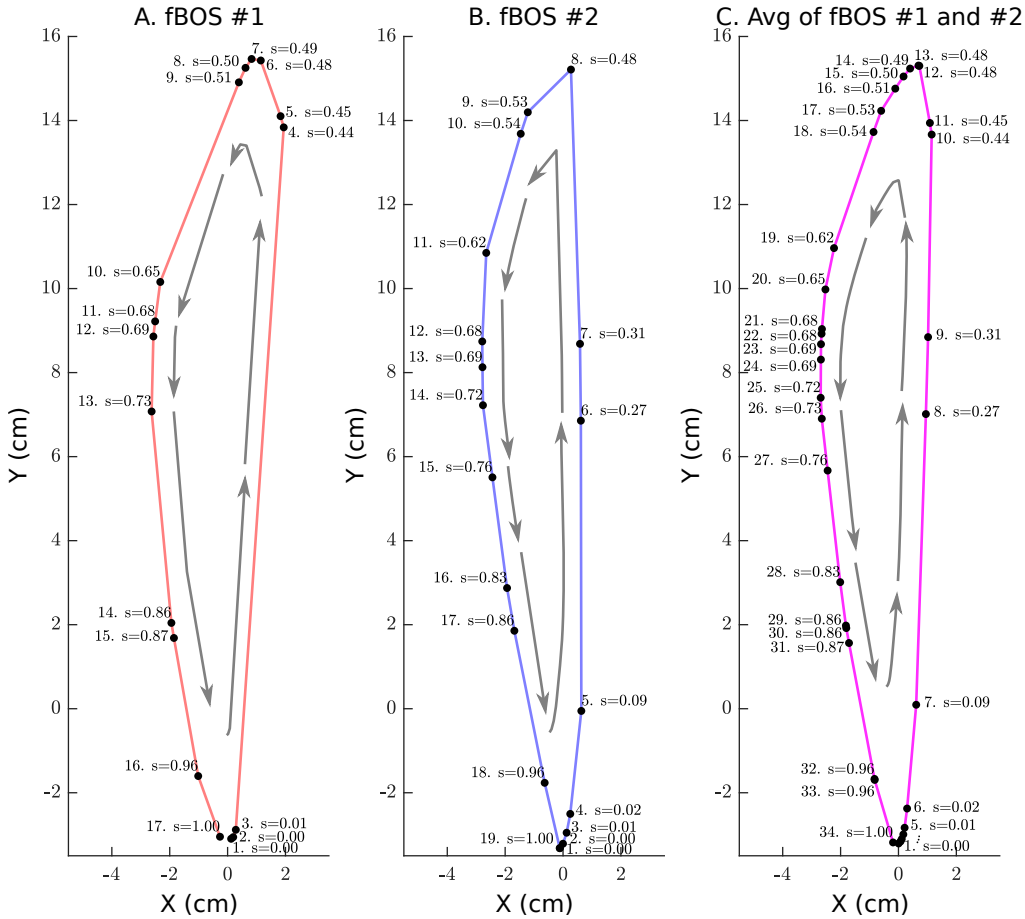

Figure C.6: An example fBOS of a foot (A) consists of 17 points while the fBOS of another foot (B) consists of 19 points. Here we use the vectors $\underline{s}_A$ and $\underline{s}_B$ to find equivalent locations between fBOS A and B. The vectors $\underline{A}_A$ and $\underline{A}_B$ contain the normalized cumulative arc-length of fBOS A and B, and $\underline{s}$ is the set of unique points in $[s_A \cup s_B]$. To evaluate the average of fBOS A and B at point s^j (C), we first linearly interpolate the $(\underline{x}_A, \underline{y}_A)$ and $(\underline{x}_B, \underline{y}_B)$ at s^j and then take the average of (x_A^j, y_A^j) and (x_B^j, y_B^j). This process is repeated across all j points in $\underline{s}$ to calculate the average fBOS (C).